THE AMERICAN SOCIETY OF MECHANICAL ENGINEERS

29 WEST 39TH STREET — NEW YORK 18, N. Y.

paper no.
56--A-124

HEAT-TRANSFER AND FLOW-FRICTION CHARACTERISTICS OF WOVEN-SCREEN AND CROSSED-ROD MATRICES

L.S. Tong
Westinghouse Electric Corp.
Commercial Atomic Power
308 Newport Road
Pittsburgh 21, Pa.

and

A. L. London, Member ASME
Professor of Mechanical Engrg.
Stanford University
Stanford, Calif.

Contributed by the Heat Transfer Division for presentation at the Annual Meeting, New York, N.Y. - November 25-30, 1956.(Manuscript received at ASME Headquarters August 1, 1956.)

Written discussion on this paper will be accepted up to January 10, 1957.

(Copies will be available until October 1, 1957)

ABSTRACT

Woven-screen or crossed-rod types of matrices may be of interest as fuel-element geometries for certain types of nuclear reactors as well as in many other heat-transfer and mass-transfer systems. Basic heat-transfer and flow-friction design data for these geometries are presented graphically, in nondimensional form, for a range of Reynolds numbers from 5 to 100,000 and matrix porosities from 0.60 to 0.83. Algebraic equations which adequately represent these data are also given and these may be used for interpolation and, at least tentatively, for a limited extrapolation beyond the range of porosities covered in this program.

3329-56

HEAT-TRANSFER AND FLOW-FRICTION CHARACTERISTICS OF WOVEN-SCREEN AND CROSSED-ROD MATRICES

By L.S.Tong and A.L.London

NOMENCLATURE

The following nomenclature is used in the paper

A	- heat-transfer area, sq ft
A_{flow}	- matrix average flow area, $A_{flow} = pA_{frontal}$, sq ft
$A_{frontal}$	- matrix frontal area, sq ft
c_p	- specific heat at constant pressure, Btu/(lb deg F)
C	- thermal capacity of copper cylinder, Btu/deg F
d	- diameter of rod and wire, in., ft
e	- base of natural logarithms, 2.718...
F	- factor defined in Equation (14)
g_c	- reciprocal of proportionality factor in Newton's second law, 32.2 (lb/#)(ft/sec^2)
G	- average mass velocity in matrix, based on A_{flow}, lb/(hr sq ft)
G_{max}	- maximum mass velocity in matrix, based on minimum free-flow area, $\sigma A_{frontal}$, lb/(hr sq ft)
h	- unit conductance for thermal convection heat transfer, Btu/(hr sq ft deg F)
k	- unit thermal conductivity, Btu/(hr sq ft deg F)
ℓ	- length of matrix in the flow direction, ft
p	- porosity of matrix, (vol of voids)/(vol of matrix)
P	- pressure, psf, or inches of H_2O
ΔP	- pressure differential, psf, or inches of H_2O
r_h	- hydraulic radius, Equations (1) and (4), ft
W	- mass-flow rate, lbs/hr

a -heat-transfer area per unit volume of matrix, Equation (3), ft^{-1}

θ -time, hr; and angle of inclination

μ -viscosity, lb/(hr ft)

ρ -mass density, pcf

σ -ratio of minimum free-flow to frontal area (=fractional opening in table 1), dimensionless

τ -wall friction drag force per unit of wall surface, psf

δ -screen thickness, $\delta = 2d_x$, in., ft

Dimensionless Groups

f -Fanning friction factor

C_D -drag coefficient per screen

N_{Pr} -prandtl number, $N_{Pr} = \mu c_p / k$

N_R -Reynolds number for tube-like flow or interior flow, $N_R = 4r_h G/\mu$

N'_R -modified Reynolds number, $N'_R = \left[(1-F_p)/F_p\right] N_R$

$N_{R(d)}$ -Reynolds number, for flow over a body, or exterior flow, $N_{R(d)} = d\, G_{max}/\mu$

N_{St} -Stanton number, $N_{St} = h/Gc_p$

x_ℓ -longitudinal pitch, ratio of longitudinal spacing to wire or rod diameter

x_t -transverse pitch, the ratio of transverse spacing to wire or rod diameter

The symbol # denotes pounds force in distinction to lb for pounds mass.

$\triangleq$ -denotes defining equation

INTRODUCTION

Matrices of the woven-screen, crossed-rod, or sphere-bed types may prove to be of interest as fuel element geometries for gas-cooled, diphenyl-cooled, and nonboiling water reactors. Fine structure matrices offer the advantages of (a) high transfer area densities, sq ft of surface/ cu ft of volume; (b) excellent heat-transfer coefficients for an acceptable flow-friction power expenditure; (c) reduced thermal stresses within the fuel element; and (d) possibly reduced fabrication costs in production quantities. Heat-transfer and flow-friction characteristics of these matrices are of interest therefore, for future reactor developments and, moreover, for more commonplace applications such as packed absorption and extraction columns; and the "periodic-flow" regenerative heat exchanger, now of interest in automotive gas-turbine application, (1)[1] and (2).

A program was started in 1949, under Office of Naval Research sponsorship, at Stanford University with the general objectives of investigating porous-body heat transfer and flow-friction behavior. The initial studies were conducted with woven-wire screen matrices, as these were capable of fairly clear-cut geometrical definition and their behavior is also of direct technical interest. A sphere-bed matrix also was included because sphere beds have served as a "standard" for the extensive flow-friction investigations of porous media. The results of this program, through 1952, are available in references (2), (3), and (4). A more recent investigation using packed steel wool was reported by Marco and Han (5).

One limitation on these earlier results, from the point of view of application to reactor fuel-element design, was that they were limited to a N_R range of about 5 to 1000. At the suggestion of the Reactor Engineering Division of Argonne National Laboratory, and with financial support from the Atomic Energy Commission, the Office of Naval Research program at Stanford was then directed to increase the Reynolds-number range up to 100,000 for the woven-screen geometry. Consumation of this objective necessitated a completely new experimental technique and test setup. The fine-woven screens ranging from 5 to 60 mesh with wire diameters from 7.6 to 41 mil were "modeled" by crossed-rod matrices composed of 0.375-in-diam rods. This increase in geometrical scale, supplemented by increased air-mass velocities, provided the desired 100-fold increase in N_R.

Because the weaving effect of the screens was not duplicated with the crossed-rod matrices, departures from complete geometrical similarity resulted. Either porosity, p, or transverse pitch x_t, could be duplicated, but not both. The decision was to duplicate porosity; and as a consequence, small corrections were applied to the crossed rod-matrix data to estimate the desired woven-screen behavior at the high Reynolds numbers. However, heat-transfer and flow-friction behavior of the crossed-rod matrices are also of technical interest. Consequently, the objectives of this paper are to report the behavior of both the woven-screen and the crossed-rod matrices in the N_R ranges from 5 to 100,000, and 300 to 100,000, respectively. Additionally, it is proposed to describe briefly

---

[1] Underlined numbers in parentheses refer to the Bibliography at the end of the paper.

the different test techniques used to achieve the low and the high N_R test ranges.

This paper constitutes a summary and condensation of reference (11).

RESULTS

The crossed-rod and woven-screen matrices are described in Table 1. The dimensions of the nominal 16-mesh, woven-screen and its associated crossed-rod-matrix model are shown in Fig. 1. The model for the nominal 24-mesh woven-screen matrix, described in Table 1, is shown in Fig. 14. For both the screen and model matrices each "screen element" was oriented at 45 deg with its neighbor so as to simulate a "random stacking" in contrast to a "regular stacking," where all the rod elements, for instance, would be either parallel or at right angles with each other.

Geometrical Parameters

The geometrical parameters used in the description of either a woven-screen or a crossed rod matrix are the porosity p, the flow hydraulic radius, r_h, the rod or wire diameter d, the transverse pitch x_t, the longitudinal pitch x_ℓ, the minimum flow-area ratio σ, and the heat-transfer area density, α. The general definition of the hydraulic radius is

$$r_h \triangleq \ell A_{flow}/A \qquad \ldots\ldots\ldots\ldots (1)$$

If one now defines an average flow area, distinct from the minimum flow area, as

$$A_{flow} \triangleq p A_{frontal} \qquad \ldots\ldots\ldots\ldots (2)$$

since by definition

$$\alpha \triangleq A/\ell A_{frontal} \qquad \ldots\ldots\ldots\ldots (3)$$

the resulting working expression for evaluating the hydraulic radius is

$$r_h = p/\alpha \qquad \ldots\ldots\ldots\ldots (4)$$

It is to be noted that both p and α can be measured or specified without ambiguity.

The sketches of Fig. 1 describe the differences between the crossed-rod and wire-matrix elements. For the idealized crossed-rod geometry shown, the following equations may be derived readily from Equations (1) to (4).

$$p = 1 - \pi/(4 x_t) \qquad \ldots\ldots\ldots\ldots (5)$$

$$\alpha d = \pi/x_t \qquad \ldots\ldots\ldots\ldots (6)$$

$$r_h/d = p/(\alpha d) \qquad \ldots\ldots\ldots\ldots (7a)$$

$$r_h/d = \left(1 - \frac{\pi}{4 x_t}\right)/\frac{\pi}{x_t} \qquad \ldots\ldots\ldots\ldots (7b)$$

$$\sigma = (x_t - 1)^2/(x_t)^2 \qquad \ldots\ldots\ldots\ldots (8)$$

Note that porosity is a function of x_t only for the crossed-rod matrix from Equation (5) and similarly for r_h/d from Equation (7b). This is not the case for the woven-screen matrix because of wire inclination due to weaving. Equations (7a) and (8) apply also to the woven-screen matrix.

Correlating Parameters

Two Reynolds numbers will be used for the purpose of correlating the flow-friction and heat-transfer characteristics

$$N_R \triangleq 4 r_h G/\mu \quad \text{and} \quad N_{R(d)} \triangleq d G_{max}/\mu \qquad \ldots\ldots (9)$$

It follows directly from the definitions

$$G \triangleq W/(p A_{frontal})$$

and

$$G_{max} \triangleq W/(\sigma A_{frontal})$$

together with Equations (7a, 7b, 5, 6) that generally for woven-wire and cross-rod matrices

$$N_R/N_{R(d)} = 4\sigma/c_1 d \qquad \ldots\ldots\ldots (10a)$$

and specifically for the crossed-rod-matrix geometry

$$N_R/N_{R(d)} = 4 (x_t - 1)^2/\pi x_t \qquad \ldots\ldots\ldots (10b)$$

The heat-transfer parameter which will be used is the conventional Stanton number

$$N_{St} = (h/Gc_p)$$

Two flow-friction parameters will be used, the Fanning friction factor

$$f \triangleq p\tau/\left\{p \frac{G^2/p^2}{2g_c}\right\} \qquad \ldots\ldots\ldots (11a)$$

and a drag coefficient

$$C_D \triangleq \frac{\delta}{r_h} p\tau/\left\{p \frac{G_{max}^2/p^2}{2g_c}\right\} \qquad \ldots\ldots\ldots (12a)$$

For essentially constant density flow

$$\tau A = \Delta P \; A_{frontal}$$

Equations (11a) and (12a) will then reduce to the more conventional "hydraulic form"

$$f = \frac{r_h}{\ell}\left(\frac{\Delta P}{P}\right)\Big/\left(\frac{G^2/\rho^2}{2g_c}\right) \qquad \ldots\ldots\ldots\ldots (11b)$$

$$C_D = \frac{\delta}{\ell}\left(\frac{\Delta P}{P}\right)\Big/\left(\frac{G^2_{max}/\rho^2}{2g_c}\right) \qquad \ldots\ldots\ldots\ldots (12b)$$

In Equation (12b) C_D is a drag coefficient, or pressure coefficient, for a single screen of thickness $\delta = 2dx_t$.

It is evident that conversion from one friction parameter to the other can be made from the general relationship.

$$\frac{f}{C_D} = \left(\frac{r_h}{\delta}\right)\left(\frac{\rho}{\sigma}\right)^2 \qquad \ldots\ldots\ldots\ldots (13a)$$

and for the crossed-rod matrix geometry

$$\frac{f}{C_D} = \frac{\left[1-\sigma/(4x_t)\right]^3}{2\left[\pi\,(x_t-1)^4/x_t^5\right]} \qquad \ldots\ldots\ldots\ldots (13b)$$

Equations (10b) and (13b) are shown graphically in Fig. 2.

As mentioned earlier, the small geometrical dissimilarity between the woven-screen matrix and the crossed-rod-matrix model prompted the selection of porosity as the common parameter. The observed behavior of the model was then "corrected" to estimate the behavior of the woven-screen matrix. The correction factors are described in the following text.

From the flow sketch in Fig. 1 it is evident that because of wire inclination due to weaving, the boundary layer develops over a longer flow length than for the crossed-rod element. A simple boundary-layer analysis indicates that the crossed-rod element would have higher heat-transfer coefficient at a given mass velocity, because of the shorter perpheral flow length for boundary-layer development. In effect, the boundary layer Reynolds number for the inclined cylinder is greater than for the cylinder normal to the flow. Thus, for the same N_{St} the effective N_R, based on r_h, for the screen matrix must be less than N_R for the rod matrix; and analysis indicated that cos θ is the factor to apply.

$$\cos\theta\ N_R\ (\text{crossed-rods}) = N_R\ (\text{woven-screen})$$

This conclusion was confirmed by tests, reported in (11), on a single cylinder at various inclinations up to 34 deg. As indicated in Table 1, the magnitudes of θ are such that this adjustment on Reynolds number is less than 12 per cent for five of the six matrices, and less than 25 per cent for the sixth. Moreover, since $N_{St} \propto N_R^{-0.375}$ approximately, even the 25 per cent adjustment has only a 9 per cent influence on N_{St}.

With this correction it was found that the low N_R screen heat-transfer behavior correlated very well with the high N_R crossed-rod test results.

From aerodynamic consideration, and also from a comparison of f/2 versus $N_{St}\ N_{Pr}^{2/3}$, the conclusion was reached that form drag provides the major contribution to friction, and that skin friction is only a minor factor. For this reason a $\cos\theta$ correction is not warranted, as for the case of heat transfer. It was then determined by trial that the direct test results of C_D versus $N_{R(d)}$, with porosity as a third parameter, provided a very good correlation of the high $N_{R(d)}$ crossed rod-matrix data with the low $N_{R(d)}$ woven-screen-matrix data. Because the model x_* did not match the woven-screen matrix x_*, this correlating procedure, in effect, resulted in a relative shift on both the friction-factor ordinate and the Reynolds-number abscissa in converting the crossed-rod matrix C_D versus $N_{R(d)}$ to f versus N_R for the woven-screen-matrix behavior. The magnitudes of these shifts is indicated in Fig. 2 by the ordinate difference between the woven-screen matrix of specified porosity and the associated crossed-rod model of the same porosity, but slightly different x_*. It may be noted that the friction factor and Reynolds-number shifts are generally small except for the p = 0.602 matrix where they are quite large.

Heat-Transfer and Flow-Friction Results

In Figs. 3 to 8 are presented the test results for six woven-screen matrices ranging in porosity from 83.2 to 60.2 per cent. The correlating factors used are, for heat transfer, $N_{St}\ N_{Pr}^{2/3}$ versus N_R, and for flow-friction, f versus N_R. In each case the lower N_R data points are from the previously reported results of Coppage, (4). The higher N_R points are corrected from the crossed-rod-matrix model data, as described previously. For heat transfer, the N_R was multiplied by $\cos\theta$ to account for wire inclination due to weaving. The friction factor f, was calculated from the model crossed-rod matrix C_D, and Equation (13a), using the woven-wire-matrix parameters (r_h, ϕ, p, and σ). There is also involved in this C_D -to-f transformation a conversion from $N_{R(d)}$ to N_R, using Equation (10a), with the appropriate woven-wire-matrix geometrical parameters.

The curves representing the heat-transfer behavior (Figs. 3 to 8) were calculated from the empirical equation.

$$N_{St}\ N_{Pr}^{2/3} = 0.375\ N'^{-0.375}_R \qquad \ldots\ldots\ldots\ (14)$$

where $N_{R'}$ is a "modified" Reynolds number as follows

$$N'_R = \frac{1-Fp}{Fp} N_R$$

$$f = 0.96 \text{ for } N'_R > 1800$$

$$f = 1.155 - 0.0601 \log_{10} N'_R \text{ for } N'_R < 1800$$

To facilitate the use of Equation (14), Fig. 10 was prepared, giving

$N'_R/N_R = (1-Fp)/Fp$ as a function of N_R.

The six heat-transfer curves from Figs. 3 and 8 and a seventh curve also calculated from Equation (14) are summarized in Fig. 9. This last curve, for a porosity of 0.390, provides a comparison with the low N_R sphere matrix data reported by Coppage and London (4). The agreement is surprisingly good, but somewhat fortuitous, because of the great difference in geometry. Moreover, Denton's results (6) for N_R from 530 to 53,000, which can be represented by

$$N_{St}\, N_{Pr}^{2/3} = 0.237\, N_R^{-0.31}$$

while forming quite a reasonable extension of the low N_R sphere data, are some 56 per cent higher than the curve from Equation (14) at $N_R = 50{,}000$. It is recommended that Equation (14) be restricted in application to either screen or crossed-rod matrices in the range of porosities of 55 to 85 per cent. Note that the application to randomly stacked crossed-rod matrices will be moderately conservative (by less than 10 per cent) because of the inclusion of the cos ϕ correction factor to account for the weaving of the screen matrices.

In Fig. 11 are presented the direct test results of C_D versus $N_{R(d)}$ for both the woven-screen and crossed-rod matrices. The generally good agreement between the low $N_{R(d)}$ behavior of the screens and the high $N_{R(d)}$ behavior determined from the rod matrices supports the adequacy of this type of correlation.

An empirical equation for this family of curves was determined to be

$$\log_{10} C_D = \frac{1.33}{p^2} N_{R(d)}^{-0.33} - \frac{0.54}{p} \qquad \ldots\ldots\ldots\ldots (15)$$

The adequacy of Equation (15) in representing the experimental results is demonstrated in Fig. 13, where the test data in the form of

$$C_D{}^p \text{ versus } p^{3.03} N_{R(d)}$$

are graphed. The agreement with the line from Equation (15), namely

$$\log_{10} C_D{}^p = 1.33 \left[p^{3.03} N_{R(d)}\right]^{-0.33} - 0.54$$

is generally within 15 per cent. Also on this graph are the results of Romie, et al (7) for three screen matrices and these data also support the correlation. Application of Equation (15), as for the heat-transfer correlation Equation (14), should be restricted to a porosity range of 55 to 85 per cent.

Because of possible interest in crossed-rod geometries for reactor fuel elements, Fig. 12 is included. Here the direct test results are presented in the form of $N_{St}\, N_{Pr}^{2/3}$ and f versus N_R. It is recommended that this representation be employed for porosities in the range 60 to 83 per cent and for N_R from 500 to 100,000 in preference to Equations (14) and (15), which were developed primarily for the woven-screen-type matrix and therefore include the small cos ϕ correction on heat transfer.

EXPERIMENTAL METHOD

The experimental method and the equipment for the low N_R characteristics are described in detail by Coppage (3). These tests were with the six woven-screen matrices described in Table 1 and one sphere matrix, porosity = 0.390, using 0.0818-in. lead balls. The friction characteristics were established by conventional steady-flow, isothermal procedures and the heat transfer by a transient technique as follows.

The matrix, initially at a uniform temperature, is heated with the air flow which, at "time zero," enters at a constant, higher temperature. The temperature-time history of the fluid leaving the matrix is recorded during this heating process. This heating curve is compared to the Anzelius and Schumann analysis of heat transfer to an idealized porous body and the convective heat-transfer coefficient is established thereby. The comparison with the theoretical solution is accomplished by matching the maximum slope of the heating curve. The reasons for selecting this procedure in lieu of other methods of comparison are discussed in reference (3).

The high N_R characteristics, obtained from tests on crossed-rod matrix models of the woven-screen matrices, were determined using the transient technique described by London, Nottage and Boelter (8) for both heat-and mass-transfer investigations and, more recently, in its application to tube banks (9) and (10).

Briefly, the technique consists of determining the time rate of cooling of a thermal capacitor of the appropriate geometry immersed in the air-flow stream. In Fig. 14, the capacitor, constructed of copper with plastic end pieces, is shown as one rod element of the matrix. Allthe other rods are of plastic. The capacitor could be withdrawn and re-inserted into the matrix at will, without interruption of the airflow.

Fig. 15 shows the section of duct containing the test matrix along with the location of the removable thermal capacitor. With the airflow established at a desired rate, the capacitor rod was withdrawn from the matrix and heated in a small electric oven 50 to 60 deg F above the duct air-flow temperature. The thermal-capacitor rod was then reinserted into the test matrix, and its temperature-time history, for the slower cooling rates, was determined with a Brown indicator, (25-in scale; 5-millivolt range; 1/2 sec full-scale response), noting the times with 1/10 sec stop watches at 1.0, 0.9, 0.8, 0.7, 0.6, and 0.5 millivolts above the temperature of the reference junction in the air stream. Thus, the test cooling range was about 15 deg F starting from about 30 deg F above the air-flow temperature. For the faster cooling rates a Brown Electronik recorder was used, with a scale setting having a sensitivity of 4 microvolts and a full-scale response of better than 1/2 sec.

The equation for the temperature of the thermal capacitor cooling in an air stream, with a pure convection resistance at the surface of (1/hA) hr F/Btu, is

$$\frac{t}{t_{\theta=0}} = e^{\frac{-hA}{C}\theta} \qquad \ldots\ldots\ldots\ldots (16)$$

where the temperatures are referred to an air-stream datum and C, the thermal capacity, is obtained from the product of mass and specific heat of the copper. For the small cooling range considered, the thermocouple emf response is linear with temperature so that the minus logarithm of the emf ratio plotted versus time yields a straight line of slope $\frac{hA}{C}$. The convective heat-transfer coefficient is calculated from this slope.

The magnitude of C/A for the thermal capacitor was about 0.40 Btu/(F sqft) (Table 1). As the range of measured h was from 3 to 100 Btu/(hr sq ft deg F) the "time constant" for the thermal resistance-capacitor circuit (C/hA), ranged from 0.133 to 0.004 hr (or about 15 sec). From this last magnitude it is clear why a recording potentiometer was required for the faster cooling runs.

For the crossed-rod matrix tests, determinations for f and C_D were made from Equations (11b) and (12b), since essentially constant density-flow conditions obtained. Because of the wide flow range, it was necessary to measure the pressure drops with either compound vertical-and-inclined draft gages, or with a 1-in-range micromanometer which had a sensitivity of 0.002 in. of water. The measured pressure drops ranged from 10 in. down to 0.01 in. of water.

As a preliminary check prior to all these tests, pitot-tube velocity traverses were made upstream from the test section in order to demonstrate uniformity of the approach flow, and also provide a check on the orifice flow meters. After suitable adjustment of the trim tabs on an egg-crate flow straightener, located upstream, $\pm$ 1 per cent uniformity over 96 per cent of the flowsection was achieved; and the orifice meter also was checked to within 1 per cent. This flow uniformity check was made at only one air rate, but since the flow was induced from the laboratory room through a smoothly converging entrance section, and the duct Reynolds number was always in excess of 30,000, the same degree of uniformity can be reasonably anticipated for the complete test range.

The estimated experimental uncertainty intervals associated with these two transient techniques are as follows (3, 11)

	Uncertainty Intervals	
	Low N_R tests, a per cent	High N_R tests, b per cent
N_{St}	$\pm$ 15	$\pm$ 3
f	5	5
N_R	2	2
N_{Pr}	2	2

a Woven-screen matrices
b Crossed-rod matrices

From the test results presented graphically in Figs. 3 to 8 and Fig. 12, it is clear that the experimental scatter and reproducibility are well within the foregoing limits. Note, however, that the foregoing estimates of experimental uncertainty do not include the speculative aspects of the corrections applied to the crossed-rod matrix behavior to predict the high N_R behavior of the woven-wire matrices. These include (a) the oblique flow, cos Θ, correction to N_R for the heat-transfer data; and (b) the relative shift in friction factor f, and N_R, reported in Fig. 2, as was suggested by the C_D versus $N_{R(d)}$ correlation of Fig. 11.

A more detailed presentation of the test equipment, the technique, and the evaluation of experimental uncertainties is contained in reference (11).

DISCUSSION

In all the tests reported in this paper the fluid used was air at approximately room temperature. As temperature differences for heat transfer were always small, variations of properties in the boundary layer were negligible. In application, however, some consideration must usually be given to the influence of fluid properties variations.

A $N_{Pr}^{2/3}$ factor is included for the Prandtl-number effect, even though this factor was essentially constant for the tests. It should be a reasonably good approximation for a N_{Pr} range of 0.6 to 3. It is not applicable for the very low Prandtl Number of liquid metals. Some limited experimental results of the influence of N_{Pr} in crossflow are discussed in a paper by Weisman (12).

Two Reynolds numbers are used in the correlations, N_R and $N_{R(d)}$, as defined by Equations (9). The first of these might be termed an equivalent tube-flow Reynolds number, as the mass velocity G is based on a porosity average flow area, and r_h characterizes a flow-passage dimension. In contrast, $N_{R(d)}$ is a parameter characteristic of flow over a body of dimension d, experiencing an oncoming mass velocity G_{max}. From the point of view of the designer, the tube flow, or interior-flow point of view is probably the most simple to apply because the dimensions r_h, p, and a are more closely related to the design problem. In contrast, for flow friction the exterior flow or aerodynamic point of view is most useful in tying together the crossed-rod and woven-screen behavior. For design convenience, after the matrix geometry is specified, it is recommended that C_D versus $N_{R(d)}$ be converted to f versus N_R, using Equations (10) and (13).

It is comforting that the f characteristic for the woven-screen geometry at the high Reynolds numbers, as predicted from the model tests, line up so well with the direct tests at the low N_R (Figs. 3 to 8). This agreement is not as strong a verification of the C_D versus $N_{R(d)}$ correlation as desired; however, because an examination of Fig. 2 will show that only the p = 0.602 matrix involves a strong enough relative shift in transferring to the f versus N_R basis. The shifts provided for the p = 0.675 and 0.725 matrices, while noticeable, are not marked enough to be really convincing. Moreover, because of the negative slope of the f versus N_R characteristic, these Reynolds numbers and f shifts are partially compensating. In effect, while the C_D versus $N_{R(d)}$ correlation of both

crossed-rod and woven-wire matrices appears to be quite promising, further confirmation for porosities in the range of 55 to 60 per cent is needed.

The correlating Equations (14) and (15) fit the woven-screen-matrix behavior very well, especially when the wide range of N_R, from 5 to 100,000 is taken into account. For heat transfer, with the exception of the N_R range below 30 for the one matrix of 0.725 porosity, the agreement is within 15 per cent. Nevertheless, it is to be strongly emphasized that while these equations are adequate for interpolating within the test porosity range, they cannot be safely extrapolated outside of the range $0.55 < p < 0.85$. In spite of this caution, because of the lack of basic design data, the engineer may be forced to make extrapolations not only to porosities outside this range, but also to other geometries. Some support for this speculative procedure, for the heat-transfer behavior, is provided by the fact that the sphere behavior on Fig. 9 is predicted quite well by Equation (14) for $N_R < 1000$ and even at a N_R = 50,000 the extrapolation provided by Equation (14) is only 56 per cent below the results of Denton (6). Comparisons of the low N_R woven-screen heat transfer are in approximate agreement with that of beds of granular materials (4).

The heat-transfer behavior for flow normal to tube banks (9), for the two staggered arrangements with a longitudinal pitch of unity, as for the crossed-rod matrices, are also in fair agreement (20 to 30 per cent lower) with Equation (14). The transverse pitch for these geometries are x_t = 2.00 and 1.50 corresponding to porosities, from Equation (15), of 0.607 and 0.477, respectively. Further comparisons of this nature are reported by Weisman (12).

The behavior reported here for crossed-rod and woven-screen matrices are for "random stacking" in contrast to "regular stacking," where the rods or wires are either parallel or at right angles with each other. For fuelelements, the "regular stacking" may prove to be more attractive from the viewpoint of fabrication. Moreover, there is some evidence to believe that the heat-transfer behavior may be improved by about 10 per cent with the same or lower friction, for the "staggered regular stacking" where flow self-shielding is not as pronounced as in either the "in-line regular stacking" or "random stacking" geometries. These questions are currently under investigation.

CONCLUSIONS

The following conclusions result from this investigation:

1 Adequate basic heat-transfer and flow-friction data are now available for the "random stacked" woven-screen and crossed-rod types of matrices, over a wide range of Reynolds numbers and a porosity range from 55 to 85 per cent.

2 The fact that two markedly different transient test techniques were employed to cover the Reynolds number range, and that substantial agreement results in the overlapping region, provides confidence in the validity of the results.

3 Extrapolation of these results to the prediction of the heat-transfer and friction behavior of other porous body geometries is risky. However, for the heat-transfer behavior at least, some limited support for this procedure is in evidence.

4 The transient technique used for the crossed-rod matrices has proved to be both simple and accurate. Wider application to other convective heat-transfer investigation is suggested.

5 For the crossed-rod matrix geometry, remaining investigations include the "regular stacked" arrays of both the "in-line" and "staggered" variety and a wider range of porosities for both the "random" and "regular stacked" geometries.

ACKNOWLEDGEMENTS

The work reported here was accomplished as part of a program at Stanford University sponsored by the USN Office of Naval Research, the Bureau of Ships, the Bureau of Aeronautics, and the AEC.

The authors are particularly appreciative for the technical assistance provided by Prof. W. M. Kays and to Mr. A. Amorosi, formerly at Argonne National Laboratory, for suggesting the program.

Stanford engineering students Mr. A. R. Ray and Mr. M. S. Shihabi assisted in the test work, calculations, and drafting.

The Harrison Radiator Division of General Motors, through Mr. John Godfrey, provided the very excellent micromanometer used for the friction factor determinations at very low pressure drops.

BIBLIOGRAPHY

1 "The Periodic-Flow Regenerator - A Summary of Design Theory" by J. E. Coppage and A. L. London, Trans. ASME, vol 75, 1953, pp. 779-787.

2 "Compact Heat Exchangers," by W. M. Kays and A. L. London, National Press, Palo Alto, Calif., 1955, pp. 19-20, 144-148.

3 "Heat Transfer and Flow Friction Characteristics of Porous Media," by J. E. Coppage, PhD Thesis, Stanford University (1952). Also issued as Stanford University Technical Report No. 16, Office of Naval Research (NR-090-104), December, 1952.

4 "Heat Transfer and Flow Friction Characteristics of Porous Media," by J. E. Coppage and A. L. London, Chemical Engineering Progress, Feb., 1956, pp. 57-F to 63-F. This is a summary of reference (3).

5 "An Investigation of Convection Heat Transfer in a Porous Medium," by S. M. Marco and L. S. Han, ASME Paper No. 55-A-104.

6 "The Heat Transfer and Pressure Loss in Fluid Flow through Randomly Packed Spheres," by W. H. Denton, C. H. Robinson, and R. S. Tibbs, HPC-35 June 28, 1949. Available through AEC Tech. Info. Div. ORNL.

7 "Heat Transfer and Pressure Drop Characteristics of Four Regenerative Heat Exchanger Matrices," by F. E. Romie, et al, ASME Paper No. 51-SA-34.

8 "Determination of Unit Conductances for Heat and Mass Transfer by the Transient Method," by A. L. London, H. B. Nottage, and L. M. K. Boelter, Industrial and Engineering Chemistry, vol. 33, April, 1941, pp. 467-473.

9 "Heat Transfer and Friction Characteristics for Gas Flow Normal to Tube Banks - Use of a Transient Test Technique," by W. M. Kays, A. L. London, and R. K. Lo, Trans. ASME, vol. 76, 1954, pp. 387-396.

10 "Average and Local Heat Transfer for Crossflow through a Tube Bank," by R. A. DeBortoli, R. E. Grimble, and J. E. Zerbe, ASME Paper No. 55-SA-51.

11 "Heat-Transfer and Friction Characteristics of Screen Matrices at High Reynolds Numbers," by Long Sun Tong, PhD Thesis, Stanford University (1956). Also issued as Stanford University Technical Report No. 28, Office of Naval Research (NR-065-104), April 1956.

12 "Effect of Void Volume and Prandtl Modulus on Heat Transfer in Tube Banks and Packed Beds," by J. Weisman, AIChE Journal, vol 1, September, 1955, p. 342.

HEAT-TRANSFER AND FLOW-FRICTION CHARACTERISTICS OF WOVEN-SCREEN AND CROSSED-ROD MATRICES

CAPTIONS FOR ILLUSTRATIONS

Fig. 1 Geometry of woven-screen and crossed-rod matrices (Dimensions are for the nominal 16-mesh screen matrix and corresponding crossed-rod model. See Table 1. Note that woven-screen matrices may have x_0 either greater or less than unity as a result of crimping or flattening respectively.)

Fig. 2 Flow-friction factor and Reynolds number ratios for crossed-rod matrices
From Equations (13b) and (10b).
+ denotes crossed-rod model conditions
e, O denotes woven-wire matrix conditions calculated from Equations (13a) and (10a).
(Ordinate differences, for a woven-wire matrix and its corresponding model, indicate the relative shift involved in converting from the C_D versus $N_{R(d)}$ correlation to predict the f versus N_R behavior of screens at high N_R shown in Figs. 3 to 8.)

Fig 3 Woven-screen matrix characteristics $N_{St}\ N_{Pr}^{2/3}$ and f versus N_R
(See Table 1 for details on the geometry. Porosity p = 0.832.)

Fig. 4 Woven-screen matrix characteristics $N_{St}\ N_{Pr}^{2/3}$ and f versus N_R
(See Table 1 for details on the geometry. Porosity p = 0.817.)

Fig. 5 Woven-screen matrix characteristics $N_{St}\ N_{Pr}^{2/3}$ and f versus N_R
(See Table 1 for details on the geometry. Porosity p = 0.766.)

Fig. 6 Woven-screen matrix characteristics $N_{St}\ N_{Pr}^{2/3}$ and f versus N_R
(See Table 1 for details on the geometry. Porosity p = 0.725.)

Fig. 7 Woven-screen matrix characteristics $N_{St}\ N_{Pr}^{2/3}$ and f versus N_R
(See Table 1 for details on the geometry. Porosity p = 0.675.)

Fig. 8 Woven-screen matrix characteristics $N_{St}\ N_{Pr}^{2/3}$ and f versus N_R
(See Table 1 for details on the geometry. Porosity p = 0.602.)

Fig. 9 Summary of heat-transfer characteristics for woven-screen matrices $N_{St}\ N_{Pr}^{2/3}$ versus N_R

(Lines are calculated from correlating Equation (14). These are the same as the lines shown in Figs. 3 to 8 for the screen matrices. Also shown is a line calculated for a porosity of 0.390 (corresponds to the porosity of a random packed sphere matrix tested by Coppage (4).)

HEAT-TRANSFER AND FLOW-FRICTION CHARACTERISTICS
OF WOVEN-SCREEN AND CROSSED-ROD MATRICES

CAPTIONS FOR ILLUSTRATIONS-Continued

Fig. 10 $N_{R}'/N_{R} = (1 - Fp)/Fp$ versus N_{R}
Supplementary graph to use with Equation (14)

Fig. 11 Friction correlation for both crossed-rod and woven-screen matrices C_{D} versus $N_{R(d)}$

Fig. 12 Crossed-rod matrix characteristics $N_{St}N_{Pr}^{2/3}$ and f versus N_{R}

Fig. 13 Test of friction correlating Equation (15)

Fig. 14 Crossed-rod matrix
(Model for p = 0.725, 24 mesh woven-wire matrix described in Table 1. Model matrix consists of 5 "screens" or 10 rows of rods. The thermal capacitor element is located in the front row of the fourth "screen" in the flow direction.)

Fig. 15 Cross-rod matrix in test duct

Table 1 Specifications for Large Scale Model and Screen Matrices

TABLE 1. SPECIFICATIONS FOR LARGE SCALE MODEL AND SCREEN MATRICES

	Model matrix I	Screen matrix 5 x 5	Model matrix II	Screen matrix 10 x 10	Model matrix III	Screen matrix 16 x 16	Model matrix IV	Screen matrix 24 x 24	Model matrix V	Screen matrix 60 x 60	Model matrix VI	Screen matrix 60 x 60
p, Porosity	0.832	0.832	0.817	0.817	0.766	0.766	0.725	0.725	0.675	0.675	0.602	0.602
d, in. Actual Dia.	0.375	0.041	0.375	0.0245	0.375	0.0175	0.375	0.0135	0.375	0.0076	0.375	0.0105
Screen Thickness, δ, in.	0.750	0.0790	0.750	0.0530	0.750	0.0335	0.750	0.0255	0.750	0.0170	0.750	0.0285
r_h, 10^{-3} ft	38.69	4.25	34.88	2.32	25.57	1.23	20.60	0.740	16.23	0.323	11.82	0.332
$x_i = \delta/2d$	1.0	0.96	1.0	1.08	1.0	0.96	1.0	0.933	1.0	1.12	1.0	1.35
x_t	4.675	4.80	4.292	4.07	3.356	3.52	2.856	3.07	2.417	2.22	1.974	1.65
a, ft^2/ft^3	21.5	196	23.4	352	29.9	624	35.2	980	41.6	2090	50.9	1820
σ, fractional opening	0.[illegible]	[illegible]	0.588	0.568	0.492	0.513	0.422	0.456	0.[illegible]	0.302	0.243	0.155
θ, degrees wire obliquity	0	11.[illegible]	0	14.6	0	15.4	0	[illegible]	[illegible]	27.0	0	41.6
length of capacitor, in.	8.56	-	8.56	-	5.00	-	5.00	-	4.441	-	4.441	-
C/A Btu/(ft^2 F)	0.391	-	0.391	-	0.396	-	0.396	-	0.395	-	0.395	-

Orientation of Model Matrix Assemblies
Nos. I, II, III: -45°, 45°, -20°, 70°, -65°, 25°, -45°, 45°, 0, 90°, -45°, 45°. 12-row matrices
IV, V, VI: -20°, 70°, -65°, 25°, -45°, 45°, 0, 90°, -45°, 45°. 10-row matrices

Location of Capacitor: Ninth-row for Models I, II, III and seventh-row for Models IV, V, VI.

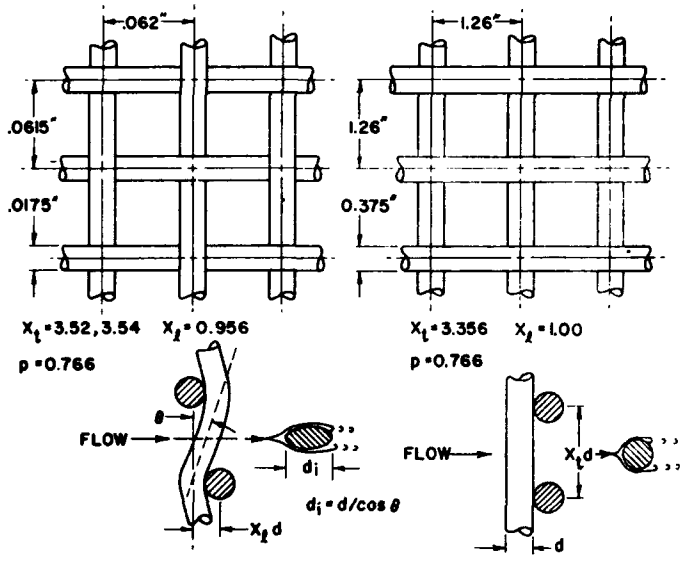

Fig.1

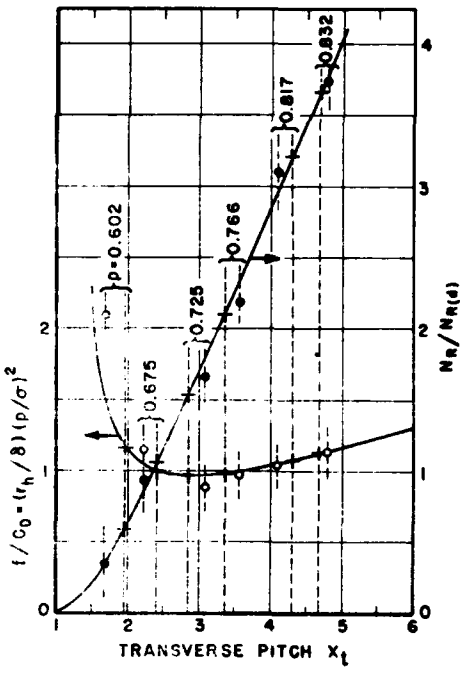

Fig.2

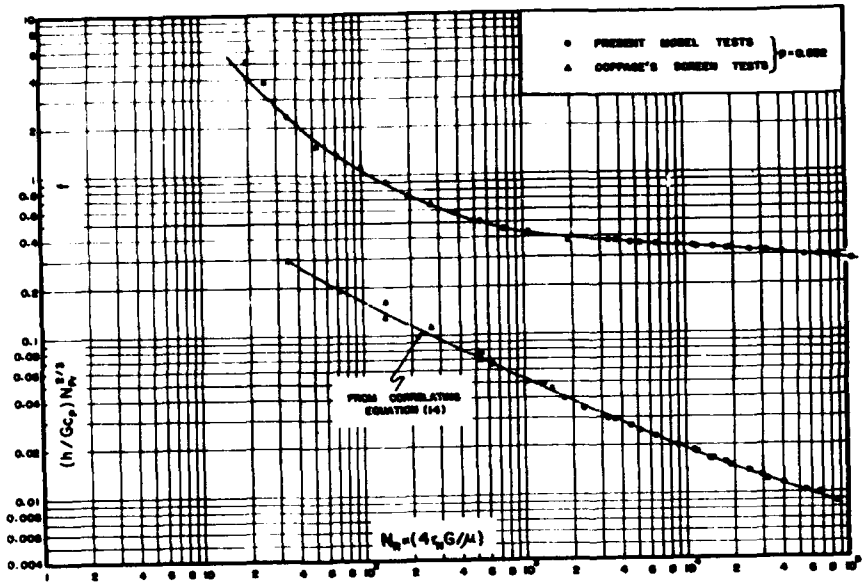

Fig.3

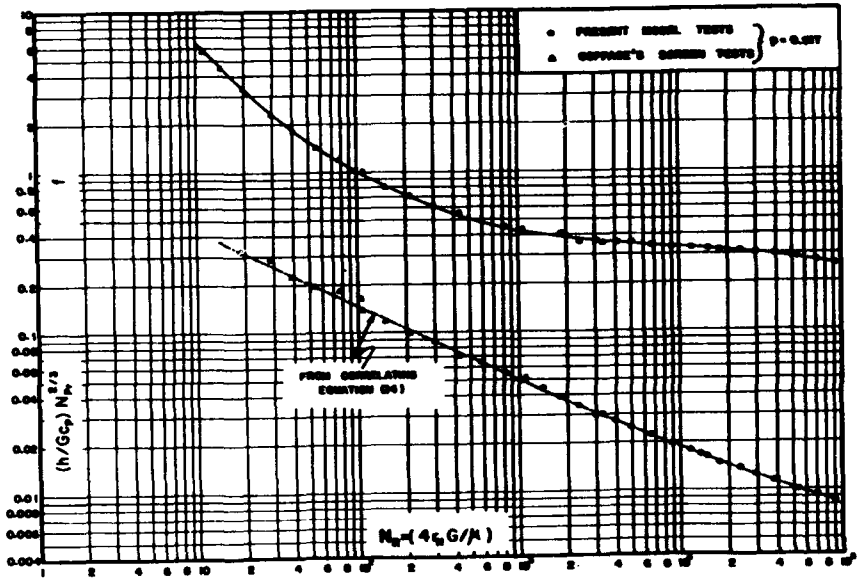

Fig.4

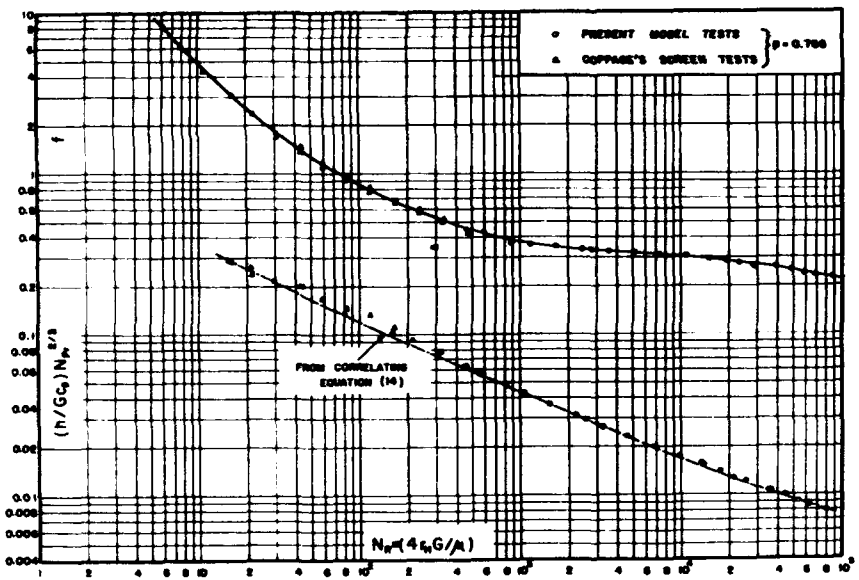

Fig.5

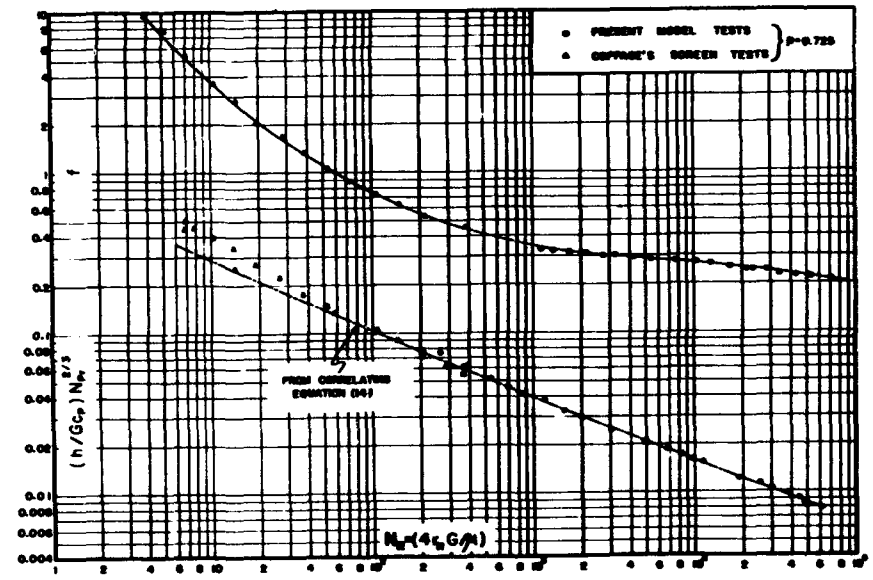

Fig.6

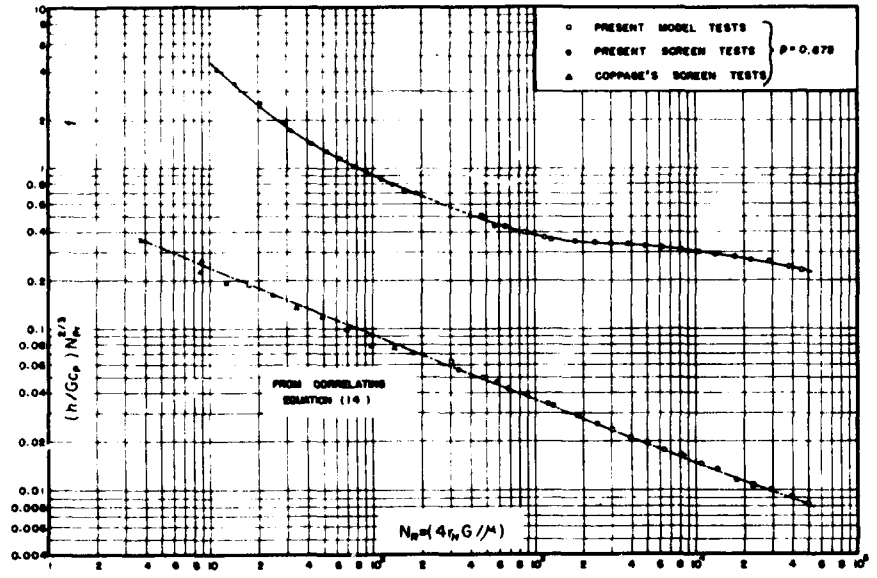

Fig.7

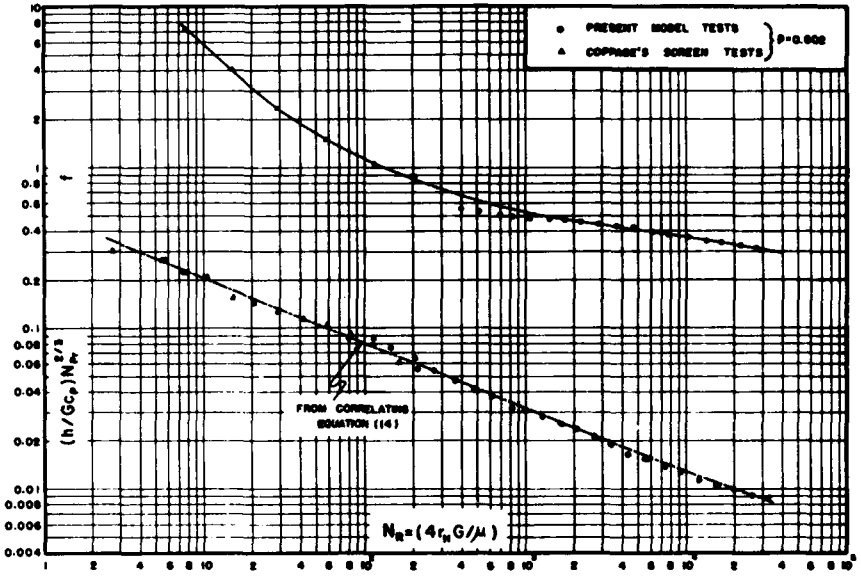

Fig.8

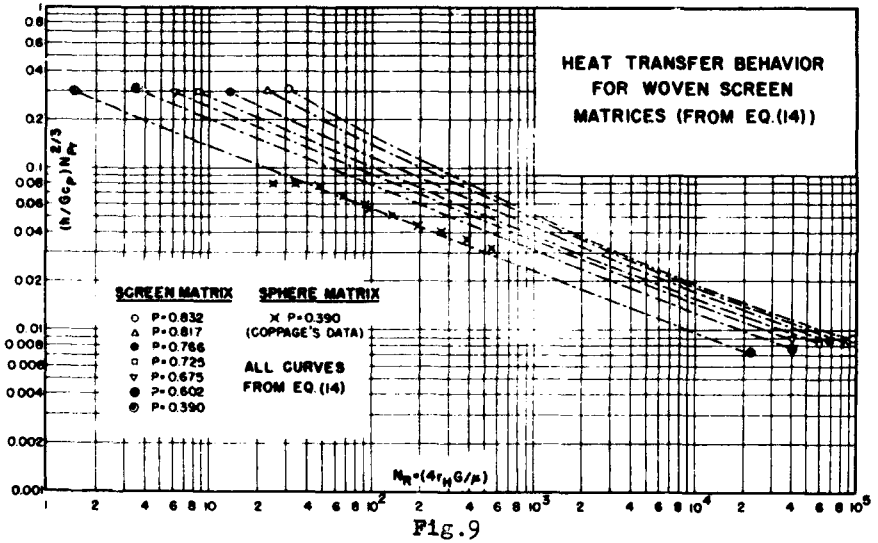

Fig.9

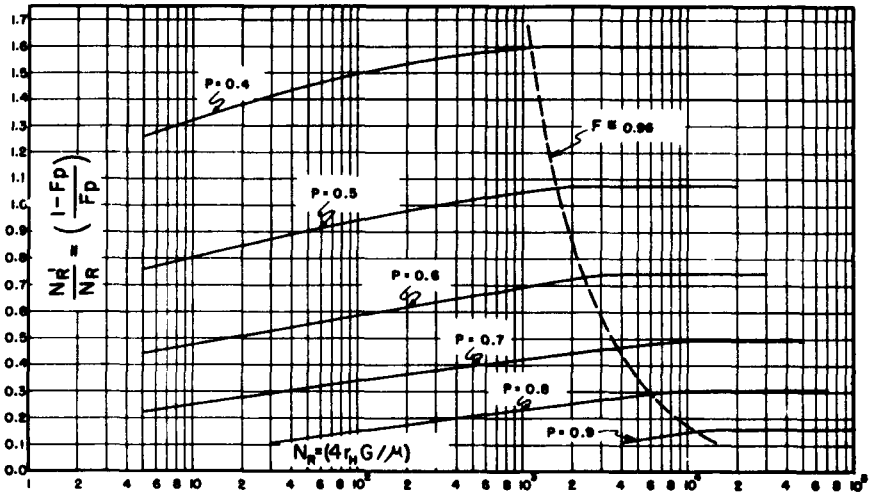

Fig.10

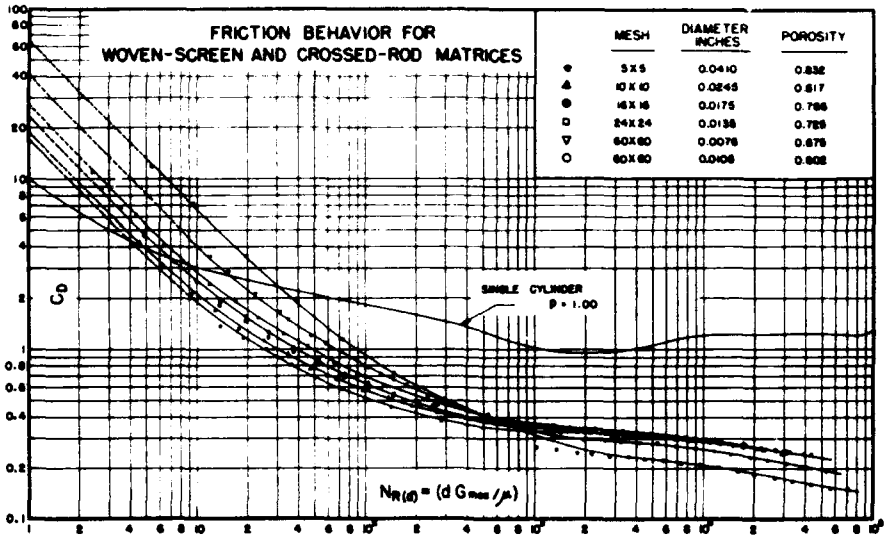

Fig.11

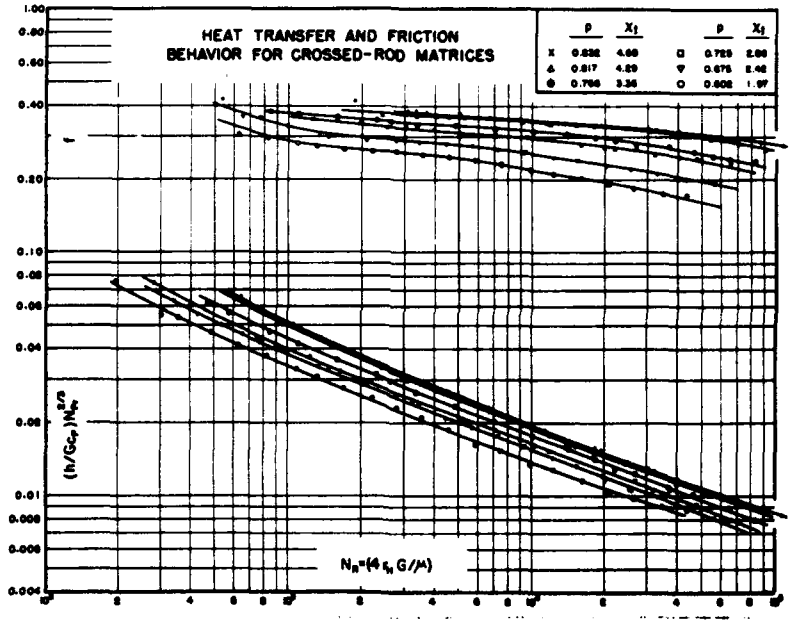

Fig.12

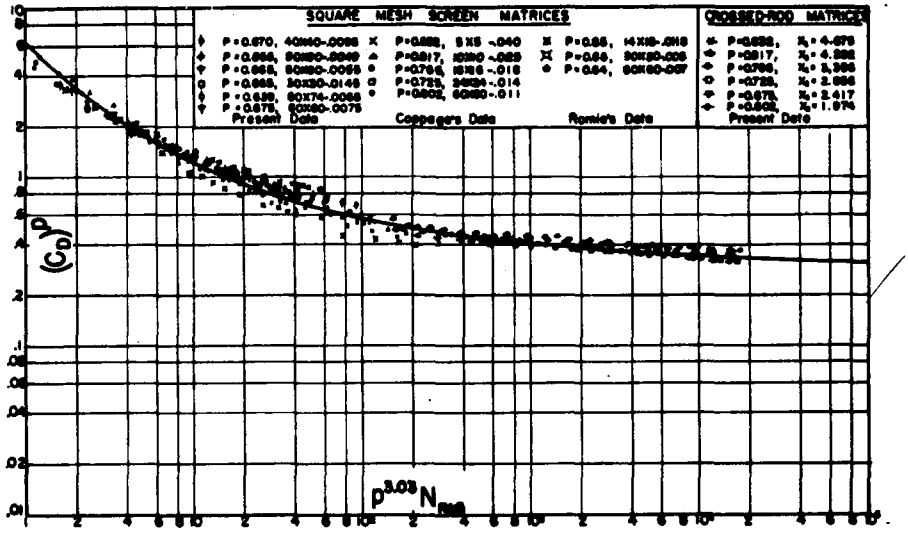

Fig.13

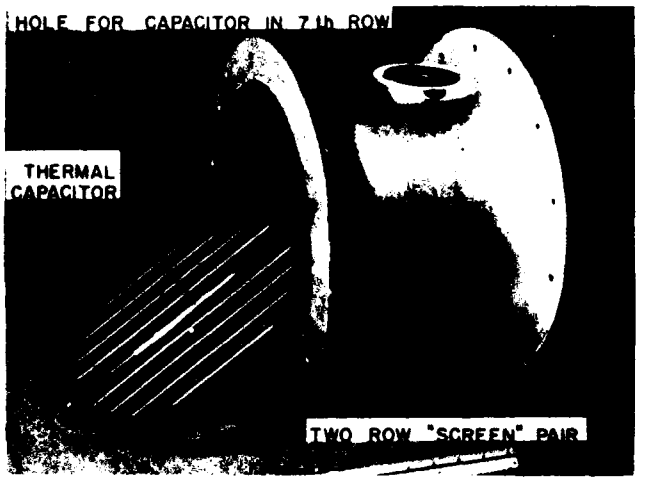
HOLE FOR CAPACITOR IN 7th ROW
THERMAL CAPACITOR
TWO ROW "SCREEN" PAIR

Fig.14

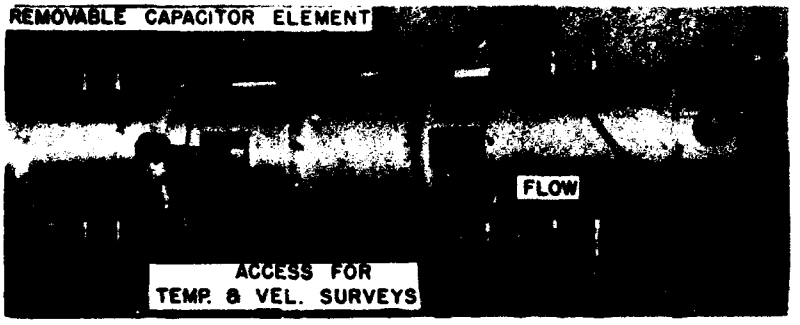
REMOVABLE CAPACITOR ELEMENT
FLOW
ACCESS FOR TEMP. & VEL. SURVEYS

Fig.15